Towards High-Speed and High-Resolution Real-Time Optical Flow Particle Image Velocimetry

Juan S. PIMIENTA[1,2], Jean-Luc AIDER[1]

1. PMMH Laboratory, UMR7636 CNRS, ESPCI Paris, PSL Research University, Sorbonne Université, University Paris Diderot, 7-9 quai Saint Bernard, 75005 Paris, France.
2. Photon Lines, 34 rue de la Croix de Fer, 78100, Saint-Germain-en-Laye, France

*Corresponding authors: juan.pimienta@espci.fr, jean-luc.aider@espci.fr

ABSTRACT

One of the major advantages of Optical Flow PIV (Particle Image Velocimetry) algorithms over Cross-Correlation PIV is their scalability leading to potentially very high computational speeds. This is confirmed in this study using different GPUs (Graphics Processor Unit) and different image sizes. The other advantage is the possibility of obtaining dense velocity fields of up to one vector per pixel. It is well known that particle seeding plays a crucial role in the results of standard particle image velocimetry based on cross-correlation algorithms. Its influence on the quality of the optical flow algorithm is not as well established. In this article the influence of particle concentration is quantified by introducing a criterion taking into account the proportion of "active" pixels in a snapshot. It is shown that it is possible to optimize particle concentration to maximize the percentage of active pixels, leading to better spatial resolution, down to one vector per pixel. The principle is validated on a vortex-free flow and applied to the complex 3D flow downstream a backward-facing step.

1. Introduction

Particle image velocimetry (PIV) is a non-intrusive technique which allows the measurement of the two components (2C) of a velocity field in a plane (2D) defined by a sheet of laser light passing through a flow of fluid seeded with reflective particles (**?**). The basic principle consists of calculating the movement of particles between two successive snapshots using, in standard PIV post-processing, an FFT (Fast Fourier Transform) cross-correlation (CC) algorithm. CC-PIV is the standard algorithm currently used in most experiments, although it is very time-consuming, computationally demanding, and limited in terms of spatial resolution or real-time measurements. To optimize the quality of the velocity fields, it is important to choose the right experimental parameters adapted to the CC algorithms, such as the time between two snapshots, leading to a maximum

displacement of a few particles inside the interrogation windows (IW), which is a key element for the spatial resolution of the PIV field (Kähler et al., 2012). However, the optimal parameters for a CC algorithm may not be the same as those for other types of algorithms, such as optical flow (OF). Indeed, OF-PIV offers a different approach. Coming from the machine vision community, optical flow can be understood as the apparent speeds of changing intensity patterns in a scene (Gibson, 1950). The general idea of estimating displacements from intensity changes is based on the assumption that intensity levels remain constant between successive images and that displacements are assumed to be small, of the order of 1 pixel.

However, determining displacement vectors from intensity variations is an under-constrained problem. This problem was solved mainly in two ways. Either a fineness constraint is imposed on the system (Horn-Schunck) (Horn & Schunck, 1981) which renders a global solution, or the displacements in the vicinity of a kernel centered on the pixels are considered very close to each other (Lukas - Kanade) (Lucas & Kanade, 1981). Later, the Lukas-Kanade OF algorithm was modified, adding it to an iterative scheme (Folki) (Besnerais & Champagnat, 2005) and then adapted to perform PIV calculations (Champagnat et al., 2011). One of the considerable advantages of FOLKI PIV is the ability to parallelize the algorithm to run efficiently on GPU (Plyer et al., 2016) and has even been optimized to run in real time (Gautier & Aider, 2013b) at the point to be used as a sensor in closed-loop flow control experiments (Gautier & Aider, 2013a, 2015). In addition to the significant gain in calculation time, OF-PIV also leads to dense velocity fields, up to 1 vector per pixel, giving access to smaller scales in the turbulent spectrum (Giannopoulos et al., 2022).

Over the last few years, the entire acquisition chain (Laser, camera, computer, algorithm) for Real-Time PIV measurement has been optimized. It leads to a high-resolution, high-frequency real-time optical flow PIV (RT-OFPIV) system. The ability to run RT-OFPIV has made possible almost unlimited observations, analysis, or recordings of large-scale instantaneous quantities derived from PIV fields. This also leads to new experimental challenges. For example, various studies and optimizations have been carried out to enhance the experimental conditions, the selection of algorithm parameters or the selection of appropriate equipment.

In the present study, we focus on the influence of seeding, and more precisely of particle concentration, on the spatial resolution of instantaneous PIV fields measured in real time. In the first part we will present the experimental setup and the performance of RT-OFPIV for both online and offline computations. We will then present a parametric study on a uniform and vortex-free flow to show the influence of seeding on the quality of the velocity fields. Finally, we will show on massively separated flows (Backward-Facing Step flow) how the improvement of the seeding allows a better resolution of the different coherent structures.

2. Experimental setup

2.1. Hydrodynamic channel

Experiments have been carried out in a hydrodynamic channel in which the flow is driven by gravity using a constant level water tank to ensure a pressure differential of $\Delta P = 0.3 \, bar$ (Fig. 1a). The maximum free-stream velocity $U_\infty = 22 \, cm.s^{-1}$ leads to a maximum Reynolds number based on the step height h of $Re_h = \dfrac{U_\infty h}{\nu} \approx 3300$ for a water temperature of $21°C$ (ν being the kinematic viscosity).

The flow is stabilized by divergent and convergent sections separated by honeycombs (Fig. 1b), leading to a turbulence intensity lower than 1 %. A NACA 0020 profile is used to smoothly start a Blasius boundary layer over the flat plate, upstream of the BFS (Fig. 2). The test section is $80 \, cm$ long with a rectangular cross-section $w = 15 \, cm$ wide and $H = 7 \, cm$ high. The height of the step h is $1.5 \, cm$ leading to a vertical expansion ratio of $A_y = \dfrac{H}{H + h} = 0.82$.

2.2. Acquisition system

To perform the PIV measurements, the water was seeded with light-reflecting polyamide microparticles $20 \, \mu m$ in diameter. The flow was ignited by a laser sheet generated by a laser beam (Coherent continuous Nd:Yag laser with a wavelength of $532 \, nm$) passing through a cylindrical Powell lens and operating at an output power of 2 Watts. Two positions for the horizontal laser sheets were used: one upstream of the BFS, in the freestream vortex-free region and the other just downstream of the BFS, near the bottom wall (Fig. 2).

To record snapshot images of the flow, a Mikrotron 21CXP12 camera was used. It can record 21 Mpx images with an acquisition frequency of up to 240 Hz.

A dedicated and personalized computer was designed and built to optimize its performance for real-time acquisition. The system is based on an AMD Ryzen Threadripper PRO 3955WX processor with 16 cores operating at a frequency of 3.90 GHz for 128 GB of RAM. Two powerful latest generation GPUs (RTX4090) are supported on a custom open chassis that allows better access and easier connection/removal of the new GPUs (Fig. 3).

3. Real-Time Optical Flow PIV

The optical flow algorithm is based on the assumption of intensity conservation between images as defined in Eq. 1):

(a)

(b)
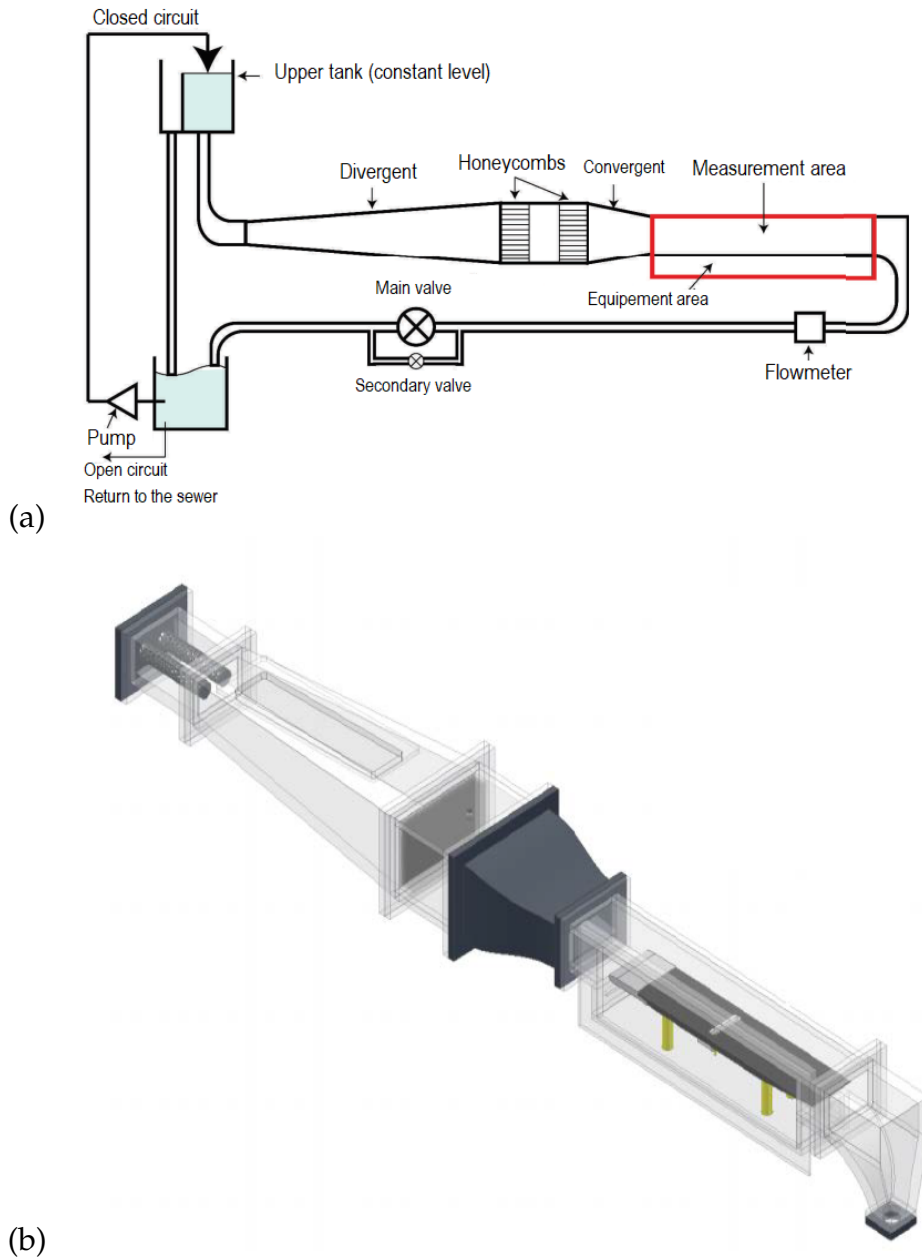
Figure 1. a) Sketch of the hydrodynamic channel. The flow is driven by gravity and stabilized using honeycombs upstream of the test section Cambonie (2012). b) 3D Sketch of test section which contains a flat plate allowing the growth of a boundary layer upstream of a BFS Gautier (2014).

$$\nabla I(x, y, t) = 0 \tag{1}$$

where $I(x, y, t)$ is the intensity measured by each pixel over time t.

By using this hypothesis and a restrictive condition it is possible to estimate the movement of the flow between two successive snapshots. The constraint imposed by the Lucas & Kanade (1981) method is to assume that neighboring pixels will behave in a similar way. This is the reason why
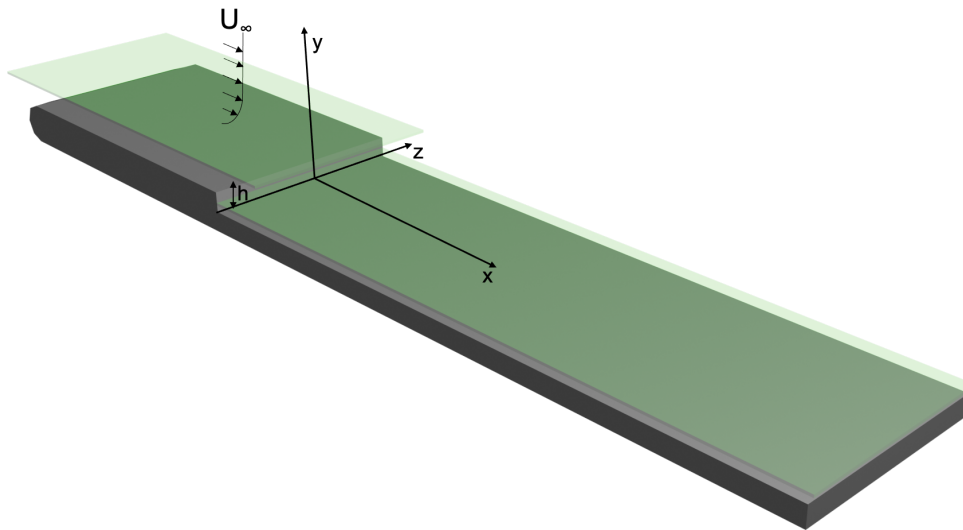
Figure 2. 3D Sketch of the BFS. The profiled plate, allowing the development of a boundary layer upstream of the BFS, is installed inside the rectangular test section shown in Fig. 1b. The optical flow measurements were carried out in two horizontal planes, one in the free-stream region upstream of the BFS and the other downstream of the BFS, relatively close to the lower wall ($y = 0.3h$).
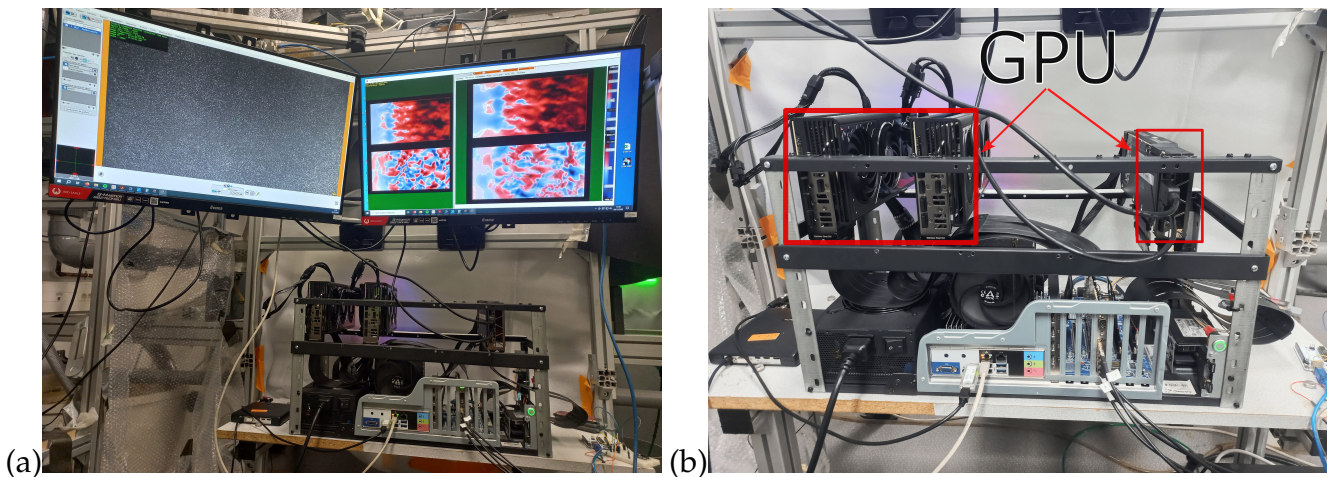
Figure 3. a) Workstation used to process PIV images in Real-Time (illustrated on the two screens). b) Close up of the workstation showing the two GPUs used for the OF computation.

FOLKI (Besnerais & Champagnat (2005)) can be considered as a compromise between pure optical flow methods and window-based methods. Indeed, it uses interrogation windows in the form of *kernels* centered on pixels, which defines one of the important parameters of the algorithm called the *kernel radius*. It defines the size of the areas where the intensity gradients will be compared. This process will be applied to each pixel, leading to a resolution of one vector per pixel.

Optical flow codes can be limited to estimate small displacements, of the order of 1 pixel. However,

this problem is solved in FOLKI by the implementation of Gaussian pyramid schemes, which make it possible to reduce the size of the image, therefore to subsample large displacements. This defines another important parameter of the algorithm called the *pyramid sublevels*. At each new pyramid level the number of pixels in each direction is halved (Fig. 4). The last important parameter of FOLKI is the number of Gauss-Newton iterations that the code must perform to give a solution. Our implementation has an additional preprocessing step before calculating the velocity fields which consists of intensity normalization using a pixel-centered kernel across the entire image.

The whole process of velocity field calculation consist in six main steps:

1 Normalization of intensity of the image.

2 Image sub-sampling with Gaussian pyramids.

3 Estimation of the displacements at the kernel scale.

4 Projection of the velocity fields up-sampling the image size.

5 Iteration through the user defined times.

6 Velocity fields estimation.

The whole process, from the two snapshots to the velocity fields computation, is presented in Fig. 4.

Even if there are general rules for choosing the right parameters (for example the number of iterations in experimental conditions rarely exceeds 4), they are strongly influenced by the characteristics of the images. For example, large displacements (more than 20 pixels between two snapshots) can be processed if the images are large enough, allowing subsampling by pyramid scheme. Nevertheless, we found that the choice of kernel radius can strongly depend not only on particle displacements, as previously thought, but also on the seeding density. Indeed, the OF principle is based on the calculation of the spatial intensity gradient in the images. If there are too many areas in the images without information, i.e. without intensity gradient, a larger kernel will be necessary. Ideally, for an OF algorithm, each pixel should provide information through a variation in intensity from one image to another. This is directly related to the concentration of particles in the flow. This point will be explained later in the discussion.

4. Performance Benchmark

To evaluate the performance of RT-OFPIV, the right parameter is the number of PIV fields calculated per second F_{PIV}, either online (Real-Time) or offline (post-processing). It is highly dependent
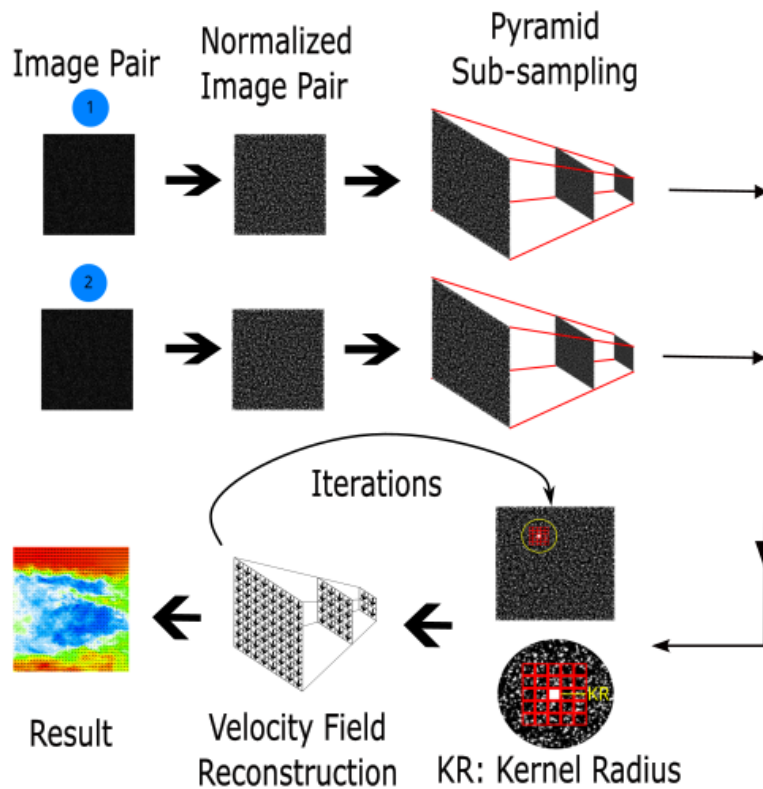
Figure 4. Workflow diagram showing the main processing steps used to compute velocity fields using Optical Flow. The Pyramid sub-sampling allows for a better estimation of all the scales present in the flow. It plays a critical role for flows with large velocity differences, like in separated flows exhibiting large free-stream velocities and slow velocities in the recirculation bubble.

on the software and hardware used for the calculations, i.e. it gives an estimate which depends on many factors such as CPU/GPU type, image size, choice of algorithm parameters and of course the streaming chain from the camera to the computer for online RT measurements. However, different configurations have been tested which give general trends in OFPIV performances.

First, the offline performance of OF calculations was evaluated on the workstation, with three different Nvidia GPUs: one RTX3090 and two different RTX4070 Ti. Additionally, a laptop equipped with an Intel Core i9-12950HX processor with 16 cores 2.30 GHz, 32 GB RAM and an NVIDIA RTX 3080Ti, was evaluated to compare with a different computer architecture. For this benchmark, synthetic images were used with a size ranging from 126×126 pixels up to 2560×2560 pixels. For all calculations the OF parameters were identical with a *kernel radius* $KR = 10$ pixels, 3 iterations, a *normalization radius* of 4 pixels and 2 *pyramid sublevels*.

Fig. 5 shows the offline benchmark result. As can be seen, the performance of the algorithm strongly depends on the size of the image. We see that it is possible to calculate velocity fields from standard 4 Mp images at a frequency between 60 and 90 Hz. 0.5 Mp image pairs can be processed at 400 Hz, while 6.5 Mp image pairs can be processed at 40-70 Hz depending on the
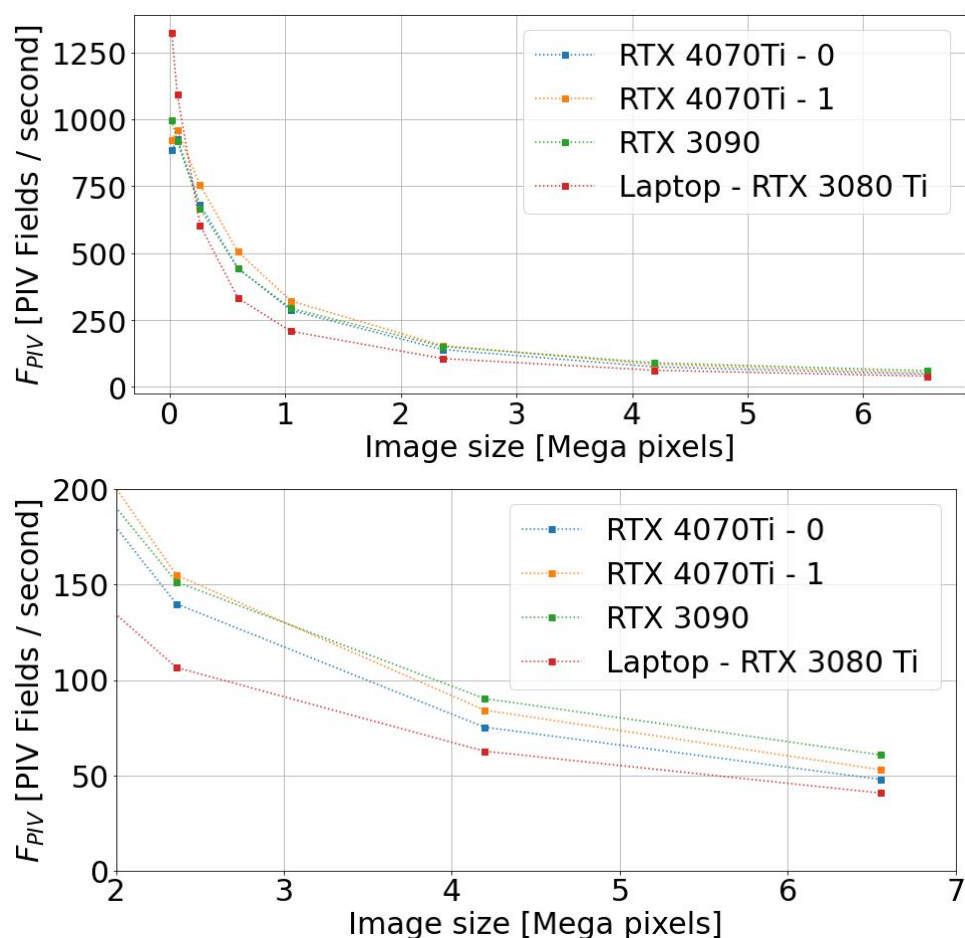
Figure 5. a) Evolution of the number of velocity fields computed per second *offline*, depending on the size of the images (in Mpixels) for four different hardware configurations. b) Zoom-in showing the number of velocity fields computed for larger images. In both cases, it shows that the performances are highly dependent of the hardware and GPUs used for the computation.

computer/GPU used. Interestingly, we found that performance is higher for smaller images when using a laptop. This can be explained by an optimized architecture optimizing communication between the CPU and GPU. Additionally, it should be noted that there may be performance differences between two identical GPUs running on the same workstation. The reason for this difference in performance between the two RTX4070 Ti is not yet understood, but it illustrates the strong dependence on the hardware used for the calculations.

The online benchmark was carried out using the Mikrotron 21CXP camera connected to the workstation via a CoaxPress card. The acquisitions are carried out on the same assembly with the same parameters. Variations in image size are made between successive acquisitions. The fields are processed in real time and processing times are recorded to compare the impact of image size on calculation times. Image sizes ranged from 1 to 21 Mp, with a dynamic range of 8 bits. The same parameters for the OF were used, as in the offline benchmark. Fig. 6 presents the evolution of the
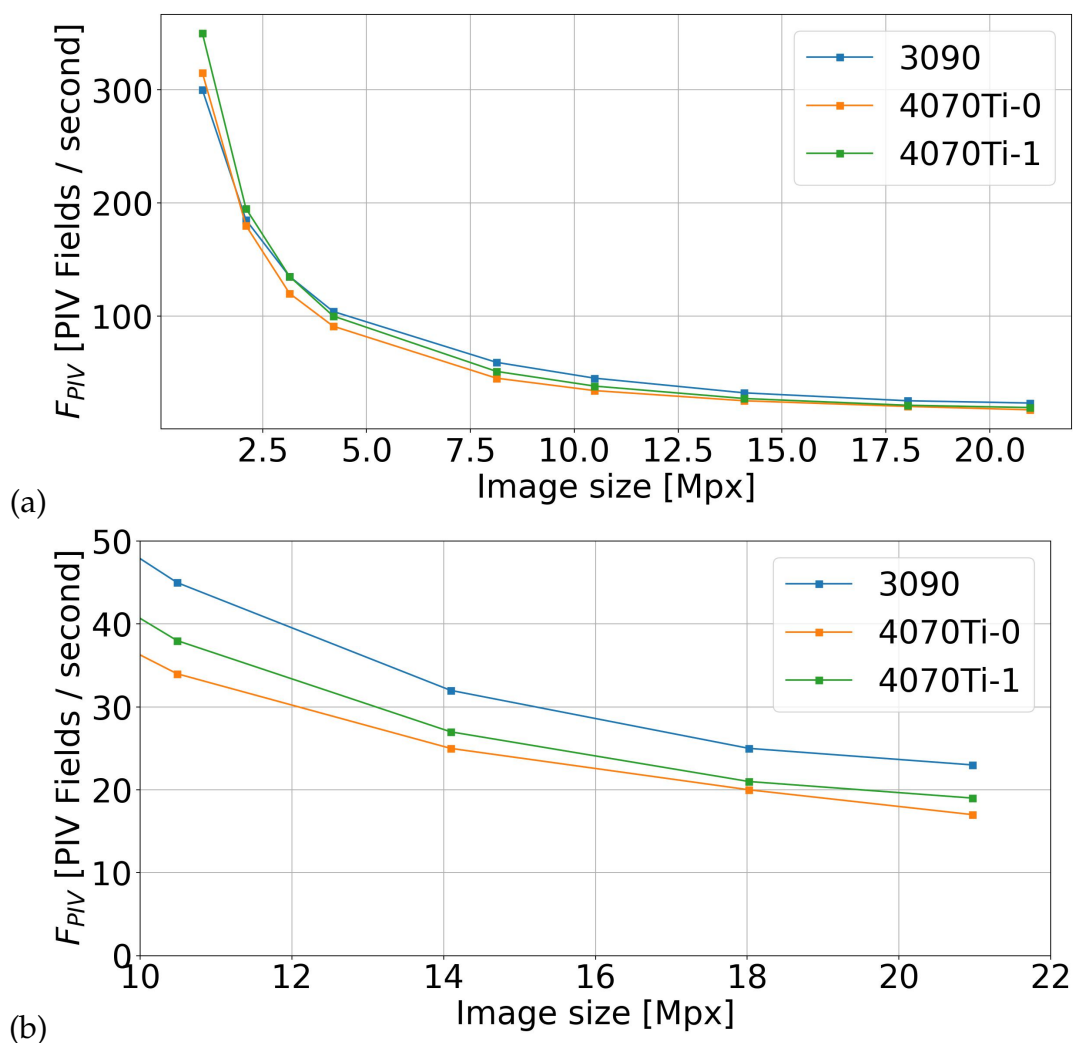
Figure 6. a) Online performance benchmark showing the Real-Time computation frequencies as a function of the image size. b) Same plot but limited to the 10 to 21 Mp images, to help seeing the variations of computing frequencies for large pictures.

real-time processing frequency as a function of the size of the images. The same trends are obtained as for offline processing. We can see that pairs of 21 Mp images can be processed in real time at 20 Hz (Fig. 6b), while standard 4 Mp images can be processed at 90 Hz. Pairs of 2 Mp images can be processed at frequencies close to 200 Hz (Fig. 6a). Surprisingly, the older GPU (RTX3090) is more efficient than the newer RTX4070 Ti GPUs for large images. The latest GPUs perform a little better for smaller images (2 Mp), also with a difference between the two identical GPUs.

5. Influence of particle seeding on the quality of the velocity fields

Given the nature of the OF algorithm, it is important to study in depth the impact of particle seeding on the quality of the results. This question is even more relevant when performing RT-

OFPIV measurements for hours, looking for low-frequency signatures in the fluctuation of scalar quantities derived from instantaneous velocity fields. Indeed, the question of seeding becomes crucial due to the sedimentation of particles over time. To avoid loss of information in the velocity fields over time, it becomes necessary to add particles into the closed-loop hydrodynamic channel. Unfortunately, a quantitative criterion is missing to know how many particles should be injected and when.
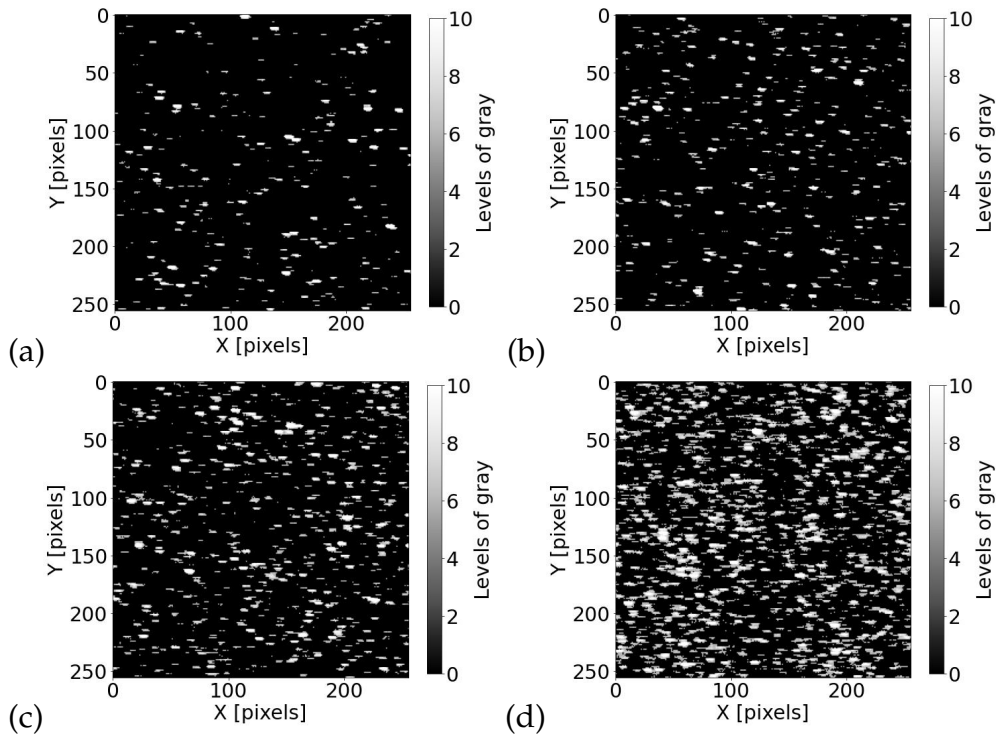

Figure 7. Sub-sample of the raw images during the change in particle concentration. a) C_0. b) $2C_0$. c) $3C_0$. d) $4C_0$

The first observation is that the standard criteria used to adjust the particle density in CC-PIV (particles per window or particles per pixel) are not adapted to OF-PIV. The appropriate criteria for OF-PIV should be related to the number of pixels *containing information relating to intensity variations*. This notion is introduced because OF works optimally when fed with a highly textured image, that is, when each pixel sees an intensity variation that can be linked to movement. Unfortunately, we can see in standard PIV snapshots (Fig. 7a) that many pixels are black and therefore do not provide any information to the OF algorithm. It becomes necessary to define quantitative criteria to optimize particle seeding in order to have the best possible texture in the images, possibly leading to better instantaneous velocity fields.

The first step consisted of increasing the concentration of particles by successive injection of 5 g of particles inside the water tank. The first injection ($C_0 = 5g$) is the standard concentration used for PIV measurements. Then, 5 g of particles were injected every 20 min while image pairs were captured every 5 s. The measurements were carried out in a horizontal plane, in the freestream and

vortex-free region, upstream of the BFS (Fig. 2). We can see in Fig. 7 the evolution of small squares of 256 pixels taken in the center of the raw snapshots to increase the concentration, showing a reduction in black pixels.
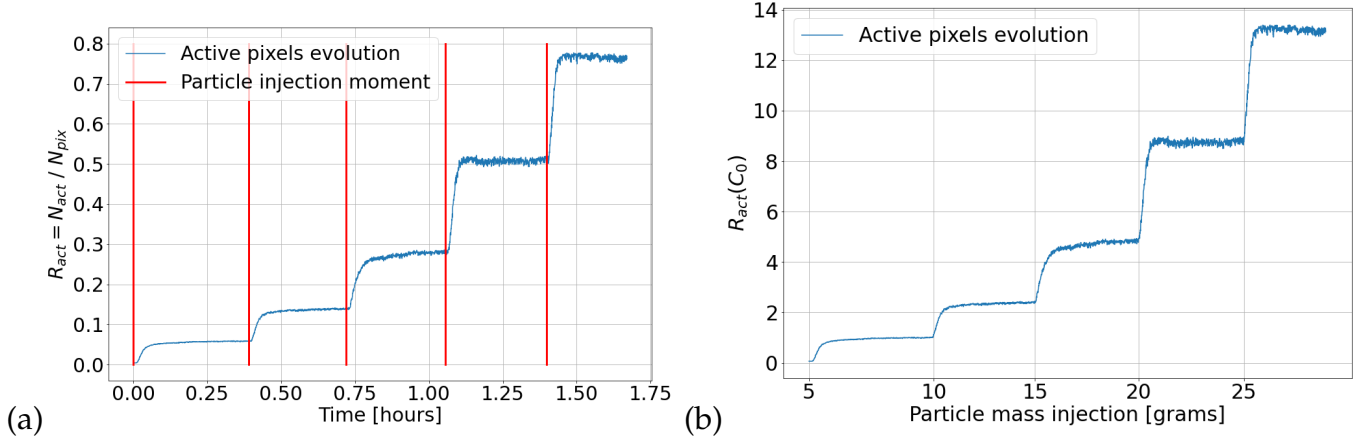
Figure 8. Evolution of percentage of active pixels for increasing concentration of particles. Each red vertical line indicate the time of a new injection of particles in the water tunnel, leading to an increase of the particle concentration.a) In terms of active pixels per image size. b) As a function of the amount of active pixels after the first particle injection C_0

In order to quantify the number of pixels containing information, we first removed the natural noise from the camera sensor, as the camera used for these acquisitions has a base noise level of 4 levels of gray when in a dynamic range of 8 bits. Next, we calculated the number of pixels N_{act} that actually detected intensity changes above the noise level. The ratio $R_{act} = N_{act}/N_{pix}$ of the number of active pixels (i.e. with information) to the total number of pixels gives the percentage of camera pixels actually containing useful information for the OF.

Fig. 8a shows the evolution of R_{act} as a function of time. Each red line corresponds to a new injection of particles, leading to an increase in the concentration of particles seen by the camera. The first observation is that for the initial concentration, only 6% of the sensor pixels contain information. This is clearly insufficient for an OF algorithm. We see that after 5 injections, leading to a total particle mass of $25g$, the ratio of active pixels increases to reach almost $R_{act} = 80\%$. Fig. 8b shows the same evolution but normalized by its value for the initial concentration $R_{act}(C_0)$ and as a function of the mass of injected particles.

This strong evolution in the proportion of active pixels should impact the quality of the resulting velocity fields calculated with the OF algorithm. Fig. 9 shows the effect of particle injection on the resulting velocity fields. We can see that the velocity field becomes denser and more homogeneous with each injection. For the maximum concentration, the velocity field becomes much smoother and uniform.

As stated previously, the kernel radius is a key parameter for OF. When dealing with suboptimal conditions for the image texture, a larger radius helps resolve the velocity estimation in a pair of

images on each pixel. But this has the side effect of losing smaller structures, because it smoothes the flow field. Using the appropriate concentration, one should obtain valuable information close to pixel resolution.
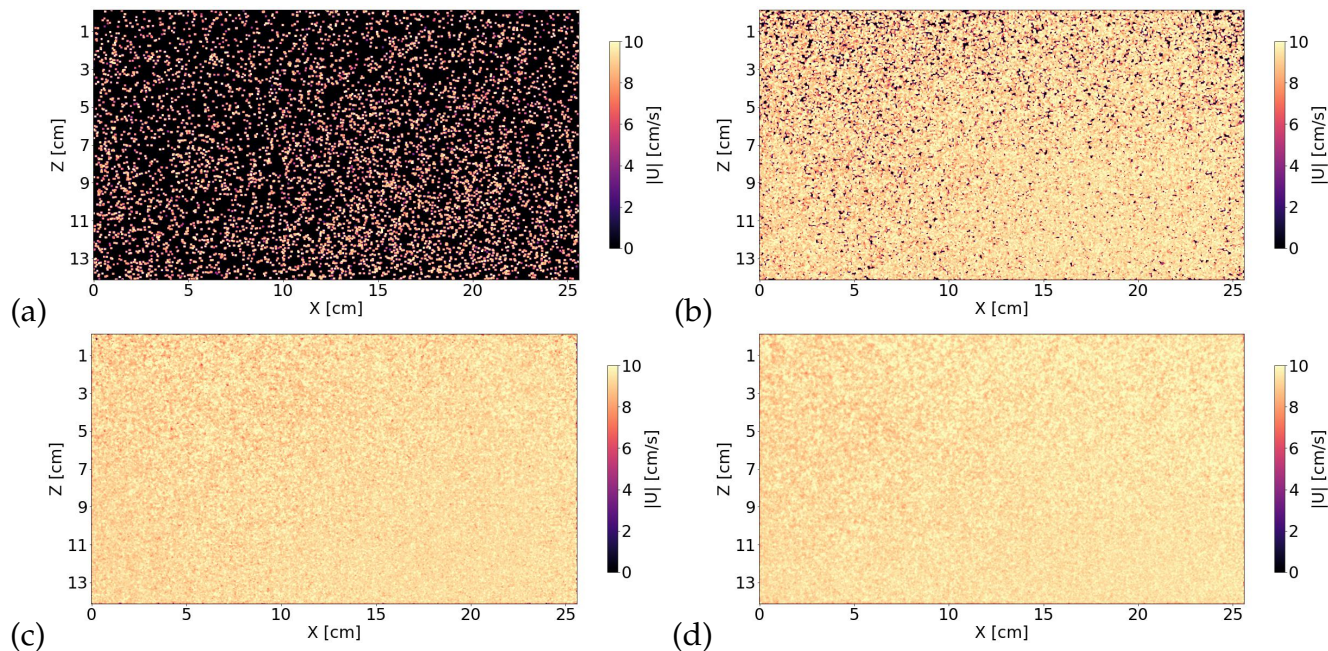
Figure 9. Impact of the number of active pixels on the velocity fields at different times. a) C_0 b) $2\,C_0$ c) $3\,C_0$ d) $4\,C_0$.

6. Influence of the concentration of particle on the spatial resolution in the velocity fields

For the next two subsections, the camera background noise was removed, as in the previous section, to improve the observation of the impact of particle seeding.

6.1. Freestream flow

In order to evaluate the impact of seeding in terms of quality of the resulting velocity fields, images in the freestream zone of the tunnel, upstream of the BFS, were taken. The objective is to calculate the velocity field of a homogeneous flow, in a region where there are no complex velocity gradients or any other 3D phenomena that might be difficult to estimate. These are the same images that were taken to characterize the quantity of active pixels in the images.

Fig. 10a presents a 2D plot of the evolution of the instantaneous velocity profile in the direction of the current, extracted from a line of pixels in the center of the image, for decreasing concentration of particles. We see that a minimum concentration is necessary to homogenize the speed profiles and obtain a good estimate of the speed. This is confirmed by Fig. 10b which shows the evolution

of the relative error made on the estimation of the speed in the direction of the flow. The error is minimized for the largest particle concentration.

Further analysis, taking into account the OF parameters, is still needed. Nevertheless, it is clear that for such a uniform flow, increasing particle seeding in the water tunnel leads to a better velocity field resolution and a reduction in noise and errors.
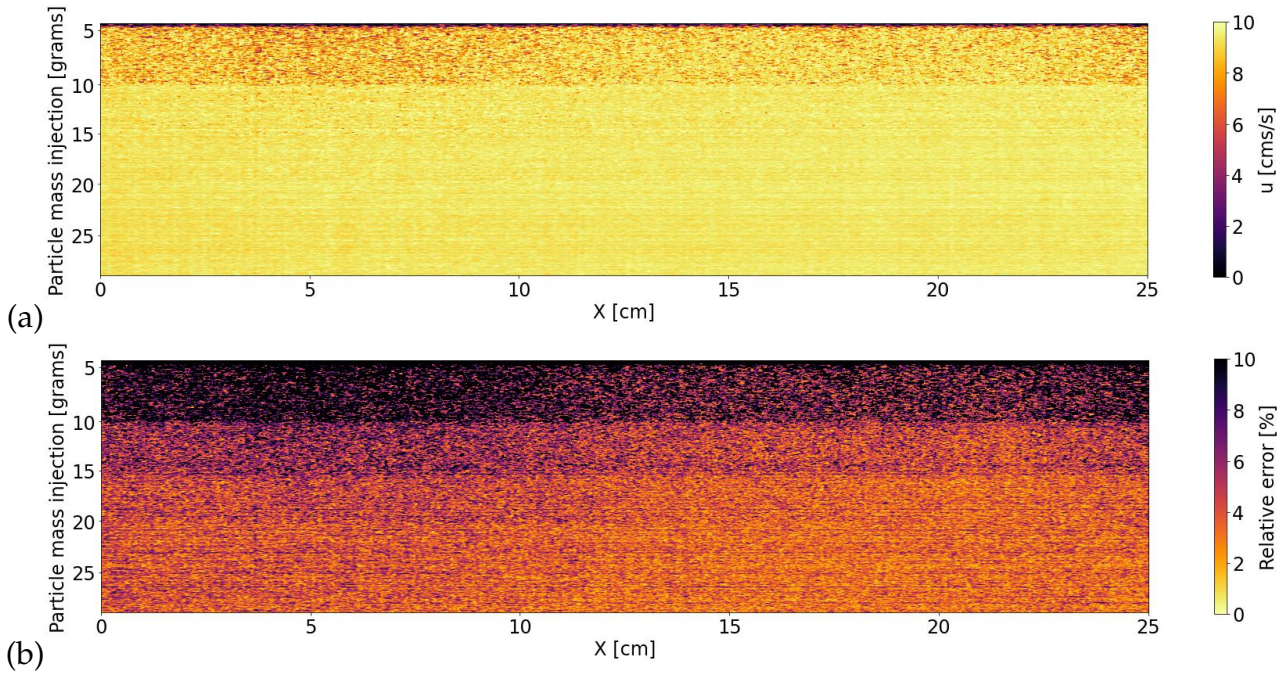

Figure 10. a) Longitudinal velocity profile at the center of the image. b) relative error of the velocity profile at the image center

6.2. Flow downstream a BFS

The same measurements were carried out downstream of a BFS in a horizontal plane, close to the lower wall (Fig. 2), in order to estimate the influence of the seeding concentration on the quality of the velocity fields. The objective is to compare the spatial resolution of the velocity fields for a flow containing many eddies of different scales. The measurements were carried out at Reynolds $Re_h = \dfrac{h \times U_\infty}{\nu} = 2040$, which corresponds to a regime close to turbulence, with strong velocity fluctuations at different scales. Two configurations are compared: one with a low particle concentration (3 g), the other with a higher concentration (25 g).

An instantaneous streamwise velocity field obtained with low concentration is shown in Fig. 11)a. It can be seen that if no smoothing is applied, some information is lost leading to holes or errors in the velocity field. It is very different when the concentration increases: there are no holes in the field which appears smooth and has fine details.
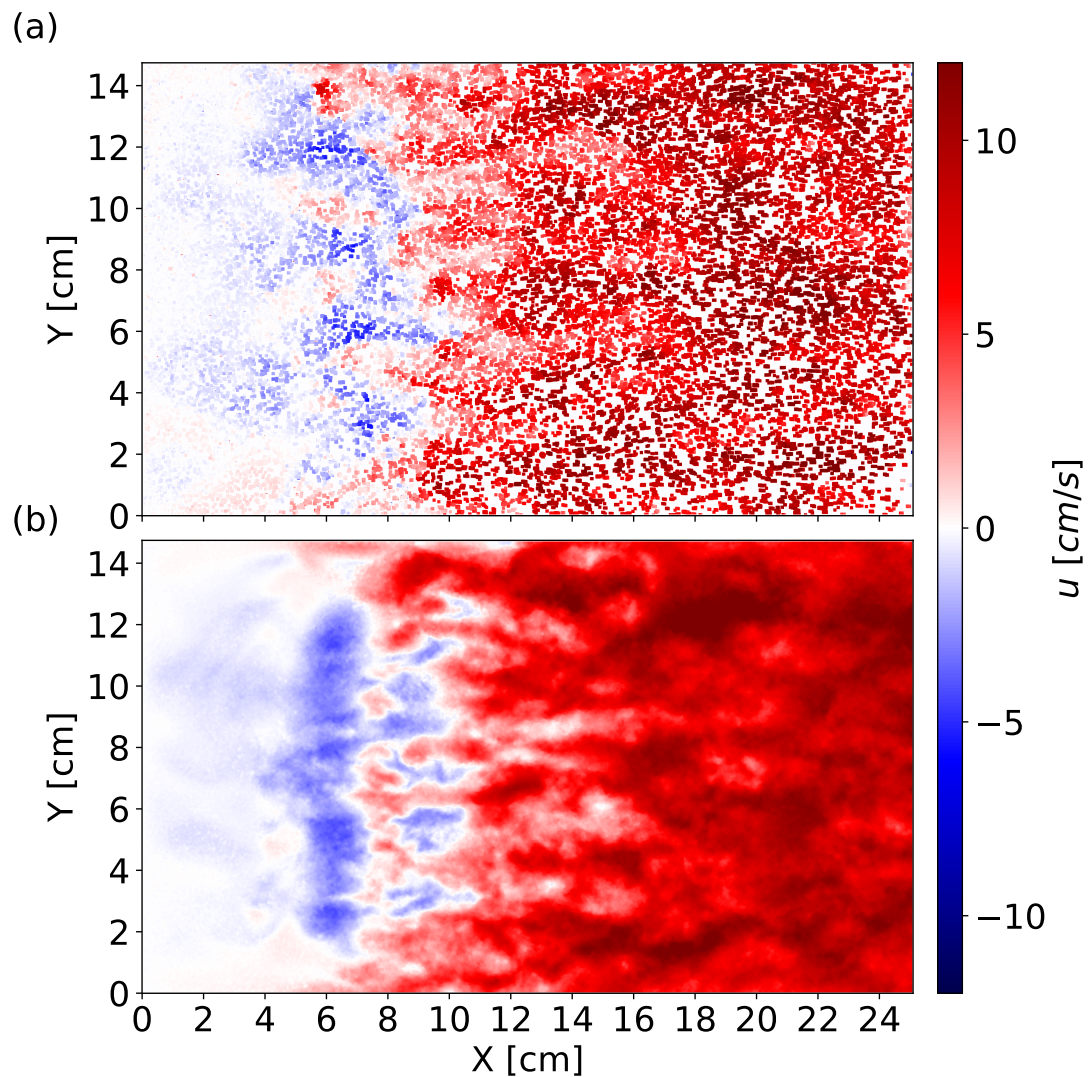
Figure 11. 2D plot of the instantaneous streamwise velocity field obtained with a low (3 *g*) concentration (a) and for a large (25 *g*) concentration (b). The qualitative difference is obvious if no smoothing is applied on the velocity fields. With a larger concentration, the instantaneous velocity field shows no hole and better definition of smaller structures.

This observation is confirmed if we plot the streamwise velocity profile along the center-line of the instantaneous velocity fields for the low concentration and the high concentration (Fig. 12). When the concentration is too low, many pixels do not contain information which leads to many zero pixels. On the other hand, it is clear that the resolution of the velocity field is improved with higher concentration. This leads to smoother velocity profiles that clearly contain valuable velocity fluctuations, without any Gaussian blur or interpolation.

It is important to note that both cases were treated with the same OF parameters: *Normalization radius* of 3 pixels, *Kernel radius* of 6 pixels, 4 *Sublevels of the pyramid* and 4 *iterations*.
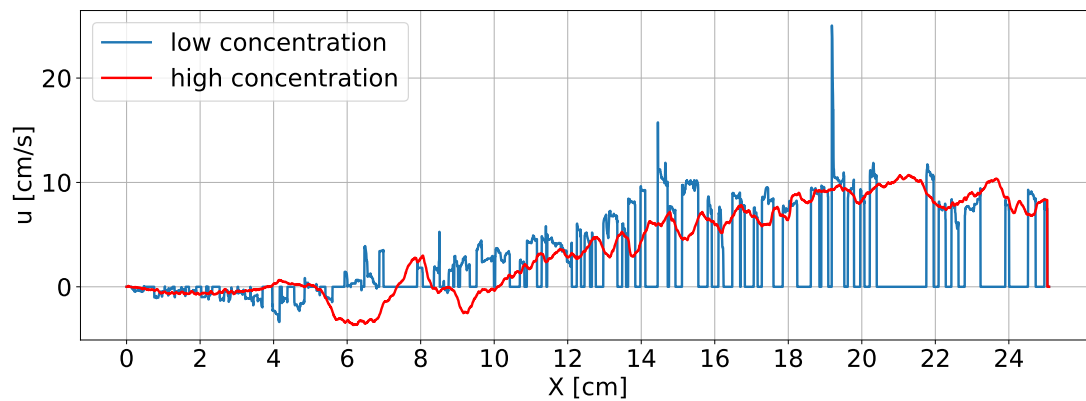
Figure 12. Streamwise profile of the streamwise component measured along the center-line of the velocity field, with a low concentration of particles (a) and a large concentration of particles (b). One can see that the profile is both smoother, without holes or sharp unphysical variations when the seeding is increased.

7. Conclusion

The objectives of the present study were to evaluate both the computational speed and spatial resolution of an optical flow algorithm. More precisely, we were interested in the influence of hardware on the calculation speed and the influence of particle seeding on the spatial resolution.

The first step was to run the OF algorithm with different GPUs on a given workstation and on a laptop with an internal GPU. The calculation speed was measured for increasing image sizes, from $0.01 \ Mp$ to $6.5 \ Mp$. The results confirmed the high efficiency of the OF algorithm. It is possible to calculate *offline* (no acquisition, use of synthetic images) velocity fields from $6.5 \ Mp$ to $60 \ Hz$, while velocity fields from $1 \ Mp$ can be calculated at nearly $300 \ Hz$. Surprisingly, the performance obtained with a laptop was as good as that of a workstation with a dedicated GPU, which is also good news because it shows that it is possible to perform RT-OFPIV measurements even with a relatively cheap setup.

The second step consisted of carrying out the same tests, but *on-line*, i.e. the calculation speed in *real time*, during the acquisition of pairs of images using a Mikrotron 21CXP camera streaming images to the workstation through a CoaxPress card. The tests were also carried out with 3 different GPUs. Results were good with all 3 GPUs. It was possible to calculate PIV fields on $21 \ Mp$ images at $20 \ Hz$ and at $100 \ Hz$ with $4 \ Mp$ images. Interestingly, the older GPU (RTX3090) was faster than the latest RTX4070 Ti when computing $21Mp$ frames, suggesting that the number of CUDA cores is the more important parameter (10496 for the RTX3090 vs 7680 for the RTX4070 Ti). It is also interesting to note that two identical GPUs do not lead to the same computing speed.

Finally, we also studied the relevance of particle seeding density on the quality and resolution of OFPIV. For this, we introduced the notion of *active pixels* as a proxy for image quality. The objective was to search for a particle seeding criterion different from the criteria used for CC-PIV, adapted to

OF. We could show that it is indeed possible to increase the number of actually useful *active pixels* in a given pair of images. Using standard seeding, well suited to CC-PIV, less than 10% of the camera sensor was used. Increasing the particle concentration led to more than 80% active pixels.

Finally, it was shown that thanks to this optimization, it was possible to increase the spatial resolution leading to better velocity fields. The measurements downstream of a BFS flow were used as a reference to evaluate the quality of the instantaneous velocity fields. 2D velocity fields obtained with lower concentration exhibit holes and errors that disappear if the particle concentration increases. Additionally, fine details associated with small structures can be observed, showing that with the appropriate parameters, OF-PIV measurements can effectively lead to dense velocity fields, with 1 vector per pixel, leading to an increase in spatial resolution. More systematic experiments are needed to confirm this result. For example, the small scales of turbulent flows can indeed be resolved in RT-OFPIV measurements, but this study demonstrates that this should indeed be possible.

References

Besnerais, G. L., & Champagnat, F. (2005). Dense optical flow by iterative local window registration. *IEEE International Conference on Image Processing 2005*, *1*, I-137. Retrieved from `https://api.semanticscholar.org/CorpusID:9992584`

Cambonie, T. (2012). *Étude par vélocimétrie volumique d'un jet dans un écoulement transverse à faibles ratios de vitesses.* (Theses, Université Pierre et Marie Curie - Paris VI). Retrieved from `https://pastel.hal.science/pastel-00795587`

Champagnat, F., Plyer, A., Besnerais, G. L., Leclaire, B., Davoust, S., & Sant, Y. L. (2011). Fast and accurate piv computation using highly parallel iterative correlation maximization. *Experiments in Fluids*, *50*, 1169-1182. Retrieved from `https://api.semanticscholar.org/CorpusID:120766529`

Gautier, N. (2014). *Flow control using optical sensors* (Theses, Université Pierre et Marie Curie - Paris VI). Retrieved from `https://theses.hal.science/tel-01150428`

Gautier, N., & Aider, J. L. (2013a). Control of the separated flow downstream of a backward-facing step using visual feedback. *Proceedings of the Royal Society A: Mathematical, Physical and Engineering Sciences*, *469*. Retrieved from `https://api.semanticscholar.org/CorpusID:118040396`

Gautier, N., & Aider, J. L. (2013b). Real-time planar flow velocity measurements using an optical flow algorithm implemented on gpu. *Journal of Visualization*, *18*, 277-286. Retrieved from `https://api.semanticscholar.org/CorpusID:9799419`

Gautier, N., & Aider, J. L. (2015). Frequency-lock reactive control of a separated flow enabled by visual sensors. *Experiments in Fluids*, *56*, 1-10. Retrieved from `https://api.semanticscholar.org/CorpusID:119779600`

Giannopoulos, A., Passaggia, P.-Y., Mazellier, N., & Aider, J.-L. (2022). On the optimal window size in optical flow and cross-correlation in particle image velocimetry: application to turbulent flows. *Experiments in Fluids*, *63*(3), 57.

Gibson, J. J. (1950). *The perception of the visual world*. Riverside Press, Cambridge, England.

Horn, B. K., & Schunck, B. G. (1981). Determining optical flow. *Artificial Intelligence*, *17*(1), 185-203. Retrieved from `https://www.sciencedirect.com/science/article/pii/0004370281900242` doi: https://doi.org/10.1016/0004-3702(81)90024-2

Kähler, C. J., Scharnowski, S., & Cierpka, C. (2012). On the resolution limit of digital particle image velocimetry. *Experiments in fluids*, *52*, 1629–1639.

Lucas, B. D., & Kanade, T. (1981). An iterative image registration technique with an application to stereo vision. In *International joint conference on artificial intelligence.* Retrieved from `https://api.semanticscholar.org/CorpusID:2121536`

Plyer, A., Besnerais, G. L., & Champagnat, F. (2016). Massively parallel lucas kanade optical flow for real-time video processing applications. *Journal of Real-Time Image Processing*, *11*, 713-730. Retrieved from `https://api.semanticscholar.org/CorpusID:10151206`